Nanocrystalline Sodalite from Al_2O_3 Pillared Clay by Solid−Solid Transformation

Sung-Reol Lee,† Yang-Su Han,† Man Park,† Gyeong-Su Park,‡ and Jin-Ho Choy*,†

National Nanohybrid Materials Laboratory, School of Chemistry and Molecular Engineering, Seoul National University, Seoul 151-747, Korea, and Samsung Advanced Institute of Technology, Post Office Box 111, Suwon 440-660, Korea

Received July 11, 2003. Revised Manuscript Received September 22, 2003

Nanocrystalline sodalite has been synthesized by a non-hydrothermal route from a solid gel mixture of Al_2O_3 pillared clay and NaOH at 80 °C. The nucleation and crystal growth mechanism for the solid−solid transformation were studied using X-ray diffraction (XRD), ^{27}Al and ^{29}Si MAS NMR, SEM, and HRTEM. Compared with hydrothermal synthesis of zeolites, the microporous Al_2O_3 pillared clay is rapidly transformed into three-dimensional zeolitic sodalite without undergoing a noticeable X-ray amorphous phase. Likewise, ^{27}Al and ^{29}Si NMR obviously reveal that the local environments around Al and Si rapidly evolve into a zeolitc Al−O−Si framework at the initial stage of reaction. Scanning electron micrographs indicate that the resulting products are composed of nanometer-sized sodalite particles (ca. 30−50 nm) with the lamellar character of pristine layered clay. HRTEM images clearly demonstrate both formations of sodalite nuclei through localized solid−solid transformation of an aluminosilicate matrix and crystal growth by rearrangement of delocalized nuclei. The results clearly explain that sodalite crystallization takes place by the solid−solid transformation without involving any solution or amorphous-mediated process.

Introduction

Zeolites are typically crystallized from amorphous aluminosilicate precursors in aqueous or nonaqueous media in the presence of alkali metal hydroxide or other strong bases.[1−3] Zeolite nuclei are supposed to form from the liquid phase and to grow into crystals by progressive incorporation of soluble nutrient species. An amorphous solid phase could serve as a reservoir of nutrients for crystal growth through gradual dissolution. Thus, the crystallization mechanism has been assumed to proceed through solution-mediated transformation.[3−5]

Recently, a great deal of effort has been directed to the exploitation of zeolite synthesis by solid−solid transformation such as dry gel conversion and molten-salt reactions, since the hydrothermal route is disadvantageous due to the requirement of excess water and the production of alkaline waste solution.[6−8] The solid−solid transformation method could lead to a much higher production yield, lower elemental losses, and shorter nucleation and crystal growth periods, compared to the hydrothermal method. Furthermore, the solid-based method also could result in smaller crystals that exhibit attractive potential applications such as zeolite membranes and catalysts.[7−8]

However, the crystallization mechanism in solid−solid transformation is not well understood. Salou et al.[6] observed that nucleation and crystal growth are much faster in the solid−solid transformation of layered silicate into silicate-1. In addition, the critical change in the solid−solid transformation reaction occurs in the initial crystal growth step, whereas that in the hydrothermal synthesis takes place during the nucleation. Serrano et al.[8] reported that the heterogeneous event in Ti-containing zeolite crystallization proceeds by the reorganization of an amorphous solid hydrogel phase in which nucleation takes place and that the crystals are formed by solid−solid transformations. Although they suggested that the crystallization of zeolite could proceed by a nonconventional mechanism accompanying the solid−solid transformation, no clear evidence has been demonstrated to explain the entire process of

* To whom all correspondence should be addressed. Phone: +82-2-880-6658. Fax: +82-2-872-9864. E-mail: jhchoy@plaza.snu.ac.kr.
† Seoul National University.
‡ Samsung Advanced Institute of Technology.

(1) Barrer, R. M. *Hydrothermal Chemistry of Zeolites*; Academic Press: New York, 1982. Breck, D. W. *Zeolite Molecular Sieves*; Wiley: London, 1974.
(2) Newsam, J. M. *Science* **1986**, *31*, 1093. Davis, M. E. *Ind. Eng. Chem. Res.* **1991**, *30*, 1675. Ozin, G. A.; Kuperman, A.; Stein, A. *Angew. Chem., Int. Ed. Engl.* **1989**, *28*, 359.
(3) Bibby, D. M.; Dale, M. P. *Nature* (London) **1985**, *317*, 157. Herreros, B.; Klinowski, J. *J. Chem. Soc., Faraday Trans.* **1995**, *91*, 1147.
(4) Madani, A.; Aznar, A.; Sanz, J.; Serratosa, J. M. *J. Phys. Chem.* **1990**, *94*, 760. Rees, L. V. C.; Chandrasekhar, S. *Zeolites* **1993**, *13*, 524. Gualtieri, A.; Norby, P.; Artioli, G.; Hanson, J. *Microporous Mater.* **1997**, *9*, 189.
(5) Mintova, S.; Olson, N. H.; Valtchev, V.; Bein, T. *Science* **1999**, *283*, 950. Davis, M. E.; Lobo, R. F. *Chem. Mater.* **1992**, *4*, 756. Dutta, P. K.; Shieh, D. C. *J. Phys. Chem.* **1986**, *90*, 2331.
(6) Salou, M.; Kooli, F.; Kiyozumi, Y.; Mikamizu, F. *J. Mater. Chem.* **2001**, *11*, 1476. Salou, M.; Kiyozumi, Y.; Mikamizu, F.; Nair, P.; Maeda, K.; Niwa, S. *J. Mater. Chem.* **1998**, *8*, 2125.
(7) Choi, C. L.; Park, M.; Lee, D. H.; Kim, J. E.; Park, B. Y.; Choi, J. *Environ. Sci. Technol.* **2001**, *35*, 2812. Afanasiev, P. *Chem. Mater.* **2001**, *13*, 459.
(8) Serrano, D. P.; Van Grieken, R. *J. Mater. Chem.* **2001**, *11*, 2391. Serrano, D. P.; Van Crieken, R.; Sanchez, P.; Sanz, R.; Rodriguez, L. *Microporous Mesoporous Mater.* **2001**, *46*, 35. Xu, W.; Dong, J.; Li, J.; Li, J.; Wu, F. *J. Chem. Soc., Chem. Commun.* **1990**, 755. Prasad Rao, P. R. H.; Matsukata, M. *Chem. Commun.* **1996**, 1441.

10.1021/cm034614p CCC: $25.00
Published on Web 11/19/2003

nucleation and crystal growth through the internal rearrangement for the solid−solid transformation. Therefore, it is essential to elucidate the solid−solid nucleation and crystal growth processes by providing direct evidence for the crystallization mechanism in the solid-based methods.

In the present study, we report the crystallization mechanism of nanocrystalline sodalite from two-dimensional aluminosilicate pillared with Al_2O_3 under extremely mild synthetic conditions. Al_2O_3 pillared clay is a suitable precursor for the sodalite crystallization because of its well-developed microporous structure and an Al/Si mole ratio similar to that of sodalite framework.[9] A detailed crystallization process is clearly elucidated by undoubtable evidence through spectroscopic and HRTEM studies along with full characterization of the resulting sodalite nanoparticles.

Experimental Section

Al_2O_3 pillared clay was prepared by the conventional ion-exchange reaction between the interlayer Na^+ ion in montmorillonite (Kunipia F, $((Na_{0.35}K_{0.01}Ca_{0.02})(Si_{3.89}Al_{0.11})(Al_{1.60}Mg_{0.32}Fe_{0.08})O_{10}(OH)_2 \cdot nH_2O$, cation exchange capacity = 100 eq/kg) and Al-polyhydroxy cation ($[Al_{13}O_4(OH)_{24}(H_2O)_{12}]^{7+}$, Keggin-type ions). The intercalated Al-polyhydroxy cations were converted to Al_2O_3 by treatment at 400 °C for 4 h in air. For conversion of Al_2O_3 pillared clay into sodalite, the pillared clay gel prepared by addition of 25 wt % water was well mixed with powdered NaOH with a typical mole ratio of $[OH^-]/[Si] = 10$. The resulting solid gel mixture was thermally treated at 80 °C under an ambient atmosphere. To investigate the transformation process under isothermal conditions, a part of the reaction product was removed periodically from the reaction mixture and used for subsequent analyses. The temperature of 80 °C was selected arbitrarily because the transformation was slow enough to allow detailed examination of the crystallization process. The products obtained at the various stages of the reaction were washed, dried, and analyzed.

Crystallinity and phase purity of the samples were determined using a Philips PW1830 automated powder X-ray diffractometer with Cu Kα radiation ($\lambda = 1.5418$ Å). The full widths at half-maximum (fwhms) of the five strongest characteristic reflections ((110), (211), (310), (222), and (411)) are used to estimate the average crystalline size by applying the Scherrer equation.

The ^{29}Si and ^{27}Al MAS NMR spectra were recorded with a 9.4 T solid-state NMR spectrometer (Bruker DSX-400). All powder samples were packed into 4-mm zirconia (Doty) rotors sealed with Kel-F end caps. The ^{27}Al MAS NMR spectra were collected in a magnetic field, $H_0 = 104.3$ MHz, with a sample spinning frequency of 14 kHz, radio frequency (rf) pulses of 0.6 ms duration, and 4-s recycle delay. The ^{29}Si MAS NMR spectra were collected at $H_0 = 79.5$ MHz with a spinning frequency of 13 kHz, a 2-ms pulse, and a 5-s recycle delay. Each spectrum was composed of 8.2 ms and 63.5 ms acquisitions. Measurements were conducted at room temperature and chemical shifts were recorded with respect to $[Al(H_2O_6)]^{3+}$ for ^{27}Al and to tetramethylsilane for ^{29}Si.

The morphology and particle size for the products were investigated by scanning electron microscopy (Hitachi S-4500) after the samples were coated with Pt/Pd alloy for 180 s with E-1030 ion sputter. HRTEM images were obtained with an FE-TEM (H-9000NA) operated at an accelerating voltage of 300 kV. The cross-sectional HRTEM specimens of the reaction products were prepared by ultramicrotome. HRTEM images were taken using a low-dose condition because the reaction products were easily damaged by the electron beam.

(9) Lee, S. R.; Han, Y. S.; Choy, J. H. *Solid State Ionics* **2002**, *151*, 343.

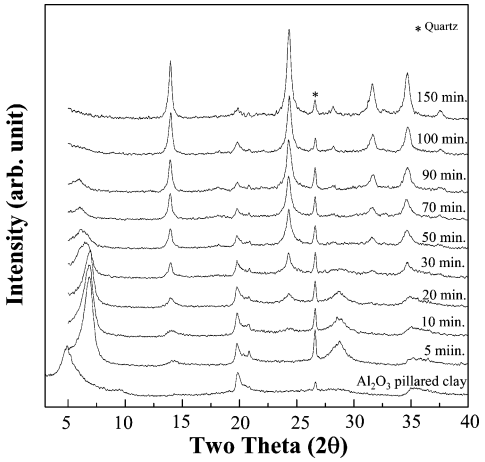

Figure 1. Powder X-ray diffraction patterns of the starting Al_2O_3 pillared clay and the reaction products obtained at the various stages of solid−solid transformation at 80 °C under an ambient atmosphere. A small amount of quartz initially present in the starting montmorillonite is always visible ($2\theta = 26.5°$) throughout the reaction.

Elemental analyses of the reaction products were carried out by atomic absorption spectroscopy (ANALAB-9100) after the samples were fused with lithium metaborate ($LiBO_2$) at 900 °C for 10 min and dissolved in a 10% nitric acid solution.

Results and Discussion

X-ray Diffraction Analysis. Figure 1 shows XRD patterns of the reaction products from Al_2O_3 pillared clay as a function of reaction time. The Al_2O_3 pillared compound exhibits a series of characteristic (00*l*) diffraction to confirm the formation of a regular intercalation compound with the basal spacing of 18.5 Å. After the solid−solid transformation reaction for 5 min, the (001) reflection of the Al_2O_3 pillared clay ($2\theta = 4.8°$, $d = 18.5$ Å) shifts to a higher 2θ angle ($2\theta = 6.4°$, $d = 12.8$ Å), indicating the collapse of interlayer Al_2O_3 pillars. After reaction for 10 min, new diffraction peaks corresponding to crystalline sodalite appear. It is worth noting here that the crystalline sodalite phase forms even within 10 min without forming any X-ray amorphous phases, which is somewhat different from the previous results in the literature.[2,10] Such a rapid formation of sodalite is surely due to the well-developed micropores of Al_2O_3 pillared clay ($S_{BET} = \sim 245$ m^2/g), which give rise to the homogeneous distribution of Si and Al. As a consequence, it provides the short diffusion paths for Si and Al atoms in the aluminosilicate network to form a sodalite framework through a solid−solid transformation without any noticeable perturbation of the pristine layer structure of montmorillonite. At the same time, the micropores in the pillared clay allow the rapid diffusion of hydrated NaOH to accelerate zeolite formation. As the reaction proceeds, the crystalline sodalite phase becomes dominant at the expense of Al_2O_3 pillared clay, and the single-phase sodalite is eventually formed after reaction for 100 min. In contrast to the conventional solution-mediated transport processes for crystal growth,[4,5] the absence of any distinct

(10) Stein, A.; Ozin, G. A.; Stucky, G. D. *J. Am. Chem. Soc.* **1990**, *112*, 904. Stein, A.; Ozin, G. A.; Macdonald, P. M.; Stucky, G. D.; Jelinek, R. *J. Am. Chem. Soc.* **1992**, *114*, 5171. Stein, A.; Ozin, G. A.; Stucky, G. D. *J. Am. Chem. Soc.* **1992**, *114*, 8119.

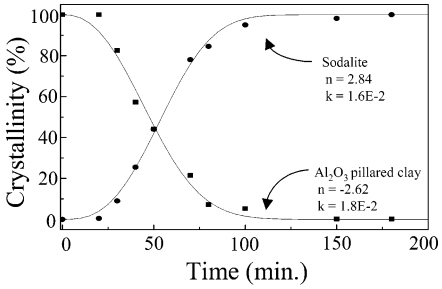

Figure 2. Crystallization and degradation curves for sodalite and Al_2O_3 pillared clay during solid−solid transformation at 80 °C. The amount of crystalline material was estimated by using integrated intensities of diffraction lines. Fitted curves from the Avrami equation are also compared (solid lines).

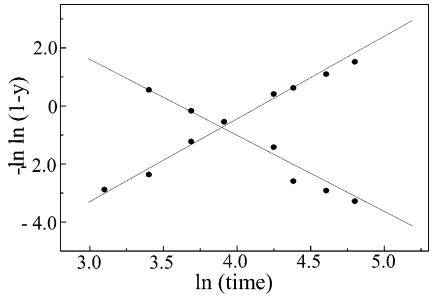

Figure 3. Data in Figure 2 plotted on a $-\ln \ln(1 - y)$ against $\ln(t)$ diagram yields values of the rate constant k (from the intercept on the y axis) and the constant n (from the slope).

X-ray amorphous stage implies that the transformation does not take place through long-range diffusion of dissolved aluminum and silicon species, but rather through a short-range molecular-level rearrangement.

To get an insight into the kinetics and crystallization mechanism involved in this transformation, the crystallization and degradation curves are extracted by normalizing the integrated intensities of the distinct diffraction peaks of sodalite (110 and 211) and Al_2O_3 pillared clay (001), respectively. Figure 2 shows the crystallization and degradation curves as a function of reaction time. In addition, the Avrami method is employed to fit the empirical kinetic curve. We consider the Avrami equation: $-\ln(1 - \alpha) = kt^n$, where α is the conversion factor, $k = d\alpha/dt$ is the rate constant, and n is the empirical parameter which describes the reaction mechanism.[11] In the logarithmic plot $\ln(-\ln(1 - \alpha))$ vs $\ln(t)$, a reaction whose kinetics conform to the Avrami equation gives a straight line in Figure 3. The line slope gives the n value. The n values are found to be 2.84 for sodalite and 2.62 for Al_2O_3 pillared clay. In the typical crystallization of zeolite with a constant nucleation and linear growth rate, the n values in the Avrami equation are expected to be around 4.[11,12] However, the n values were often found to be significantly greater than 4, especially when the starting materials were amorphous metakalonites ($n = 5-7$).[12] High n values have been explained by the autocatalytic nucleation effect. On the other hand, when the n value is less than 4, the crystallization does not involve formation of significant amounts of amorphous phase and autocatalytic nucleation.[11] Such low n values also strongly suggest that a solid−solid transformation process occurs without involving any intermediate amorphous phase, and, if any, only a small fraction of the starting materials might undergo an amorphous phase.

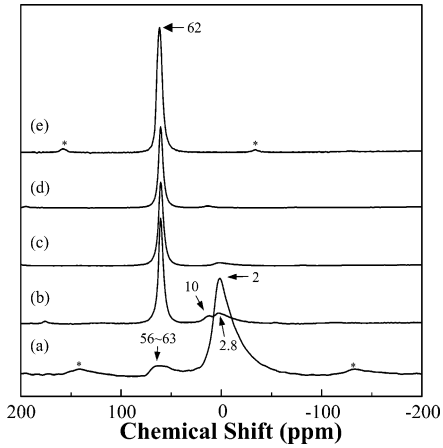

Figure 4. ^{27}Al MAS NMR spectra during the solid−solid transformation of Al_2O_3 pillared clay (a) into sodalite at 80 °C under an ambient atmosphere: (b) 30 min; (c) 50 min; (d) 100 min; and (e) 150 min; * indicates spinning sidebands.

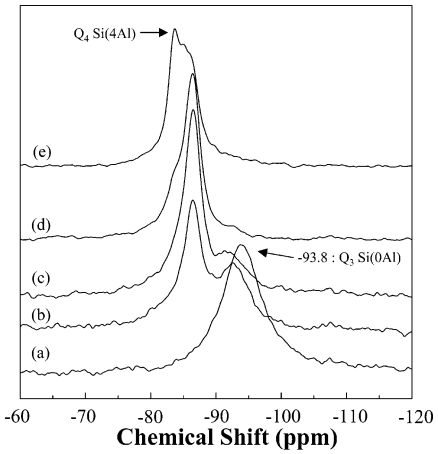

Figure 5. ^{29}Si MAS NMR spectra during the solid−solid transformation of Al_2O_3 pillared clay (a) into sodalite at 80 °C under an ambient atmosphere: (b) 30 min; (c) 50 min; (d) 100 min; and (e) 150 min.

^{27}Al and ^{29}Si MAS NMR. The evolution of local environments around Al and Si atoms during transformation was investigated by ^{27}Al and ^{29}Si MAS NMR spectroscopy (Figures 4 and 5). After a reaction time of 30 min, when the sodalite phase is detected by the XRD analyses, new narrow resonance lines at 62 ppm in ^{27}Al spectra and at −86.5 ppm in ^{29}Si spectra appear at the expense of the peaks related to Al_2O_3 pillared clay. The isotropic chemical shift of Al ($\delta_{Al} = 62$ ppm) is characteristic of the tetrahedral Al in sodalite with Si/Al = 1, while that of Si ($\delta_{Si} = -86.5$ ppm) is unambiguously assigned to the Si(4Al) of sodalite with a perfect alternating ordering of the Si and Al tetrahedrons,[13−17] which is supported by the Si/Al molar ratio

(11) Putnis, A. *Introduction to Mineral Sciences*; Cambridge University Press: New York, 1992. Norby, P. *J. Am. Chem. Soc.* **1997**, *119*, 5215.

(12) Thompson, R. W.; Dyer, A. *Zeolites* **1985**, *5*, 202. Gualties, A.; Norby, P.; Artioli, G.; Habson, J. *Phys. Chem. Miner.* **1997**, *24*, 191.

(13) Woessner, D. E. *Am. Mineral.* **1989**, *74*, 203. Klinowski, J. *Chem. Rev.* **1991**, *91*, 1459.

(14) Fitzgerald, J. J.; Piedra, G.; Dec, S. F.; Seger, M.; Godber, G. E. *J. Am. Chem. Soc.* **1997**, *119*, 7832.

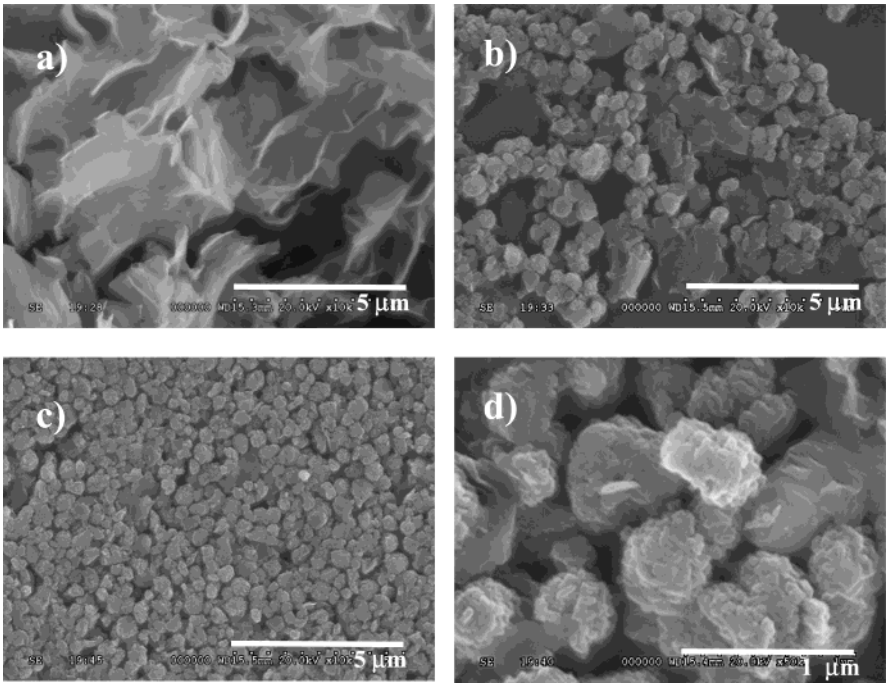

Figure 6. Scanning electron micrographs of the Al_2O_3 pillared clay (a) and the solid products obtained at different stages of the transformation at 80 °C: (b) 30 min; (c) 150 min; and (d) the enlarged morphologies of the product shown in (c).

measured from elemental analysis. This result implies that the local environments around Al and Si atoms are rapidly changed to a zeolitic Al−O−Si tetrahedral network at the beginning of the reaction. At the same time, the resonance peak due to Al(VI) in octahedral coordination is drastically reduced in intensity and resolved into two peaks with $\delta = 2.8$ and 10 ppm, respectively. From the observed chemical shift, the peak at 10 ppm can be assigned to hydroxide-type aluminum compounds such as $Al(OH)_3$ or AlOOH derived from the Al_2O_3 pillars.[14] The resonance line due to the tetrahedral Al becomes significant with the reaction time, while the resonance line associated with octahedral Al becomes negligible even after 30 min and disappears completely after 150 min. The main Si NMR peak of the product obtained after 150 min shows a low field shift to $\delta = 84$ ppm along with two separated shoulders at 86−87 ppm. Typically, the change in the chemical environments, such as the number of tetrahedral Al atoms near Si atom, leads to the shift more than $\Delta\delta = \sim 5$ ppm.[13] Therefore, both the field shift and the peak separation seem to result from the effect of the species encapsulated in the cavity rather than from the change in the coordination environment because the overall shift takes place within $\Delta\delta < 4$ ppm.[17] The exact assignment to the fine splitting needs more detailed structural analysis. Additionally, no distinguishable changes in chemical shift and in full width at half-maxima (fwhm: 5−6 ppm) are observed, supporting again the view that the local symmetry of Al atoms is already determined at the initial stage of the reaction.[15]

Electron Microscopy Studies (SEM). The evolution of crystal morphology and particle size during the solid−solid transformation was investigated by scanning electron microscopy (Figure 6). According to the SEM image for the starting Al_2O_3 pillared clay, a porous and platelike morphology could be observed. After being transformed for 30 min, small spherical shapes appeared at the surface of the platelike particles, indicating that sodalite crystals are grown at the expense of the Al_2O_3 pillared clay particles. It becomes more evident from the enlarged SEM micrograph (Figure 6d) that the crystalline sodalite particles emerge from the lamellar aluminosilicates, indicating that the reaction occurs topochemically. Moreover, the spherical particles (∼500 nm) are composed of extremely small crystalline sodalites with a size of 30−50 nm diameter, which is well consistent with the average crystalline size evaluated by the Scherrer equation with the five strongest peaks of XRD. As the reaction proceeds, the spherical aggregates consisting of sodalite nanocrystals become dominant instead of lamellar Al_2O_3 pillared clay. Even though the number of sodalite particles increases with reaction time, the dimensions of the spherical aggregates (secondary particles), as well as the primary sodalite crystals, are quite constant in size. This is an indication that the crystallization of sodalite takes place mainly by the solid−solid transformation in a limited dimension, which results in the sodalite nanocrystals.

Solid−Solid Transformation Mechanism (HRTEM). Sodalite formation through the solid−solid transformation is clearly visualized by high-resolution transmission electron microscopy (HRTEM). Figure 7 a shows typical HRTEM images of a thin-sectioned Al_2O_3 pillared clay oriented with its *ab* planes parallel to the optical axis of the microscope. The clay layers are discernible as solid dark lines while the pores appear in light contrast between layers. After reaction for 30 min (Figure 7b), a new lattice fringe of sodalite appears

(15) Rocha, J.; Klinowski, J.; Adams, J. M. *J. Chem. Soc., Faraday Trans.* **1991**, *87*, 3091. Akolekar, D.; Chaffee, A.; Howe, R. F. *Zeolites* **1997**, *19*, 359.

(16) Fripiat, J. J. *Catal. Today* **1988**, *2*, 281. Weiss, C. A.; Altaner, S. P.; Kirkpatrick, R. J. *Am. Mineral.* **1987**, *72*, 935.

(17) Lippmaa, E.; Magi, M.; Samoson, A.; Tarmak, M.; Engelhardt, G. *J. Am. Chem. Soc.* **1981**, *103*, 4992. Engelhardt, G.; Felsche, J.; Sieger, P. *J. Am. Chem. Soc.* **1992**, *114*, 1173.

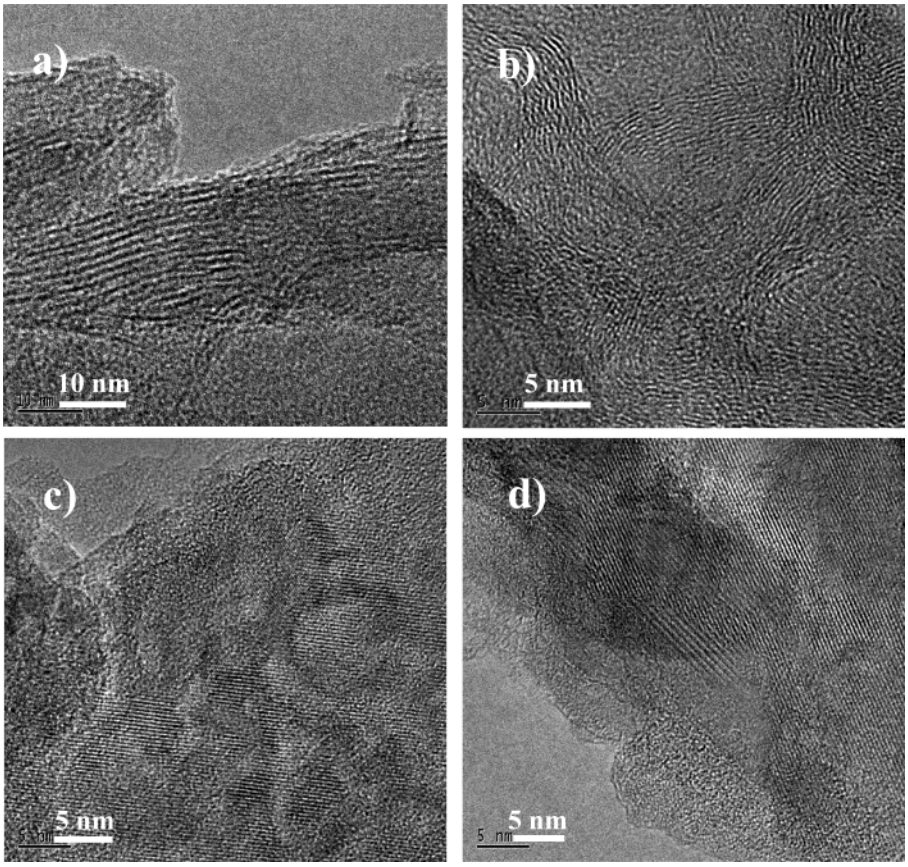

Figure 7. HRTEM images of Al_2O_3 pillared clay (a) and the solid products obtained by solid−solid transformation: (b) 30 min; (c) 100 min; and (d) 150 min.

randomly in the crystalline region. The formation of highly delocalized lattice fringes of sodalite is eventually rearranged into a well-developed lattice with respect to the reaction time, which highlights the course of crystal growth by rearrangement of delocalized nuclei. The process leads to the long-range lattice fringes of sodalite. As the reaction proceeds, the long-range lattice fringes become dominant instead of the dislocated lattice phases. Figure 7d shows the fully crystalline lattice fringes of sodalite obtained after 150 min. HRTEM images clearly demonstrate that the formation of sodalite nuclei takes place simultaneously from an aluminosilicate matrix by the solid−solid transformation of an entire clay lattice, and that a rapid crystal growth takes place through the rearrangement of sodalite nuclei with a limited dimension to result in nanocrystalline sodalite with a discrete particle size distribution. This result is well consistent with the SEM observation.

Conclusions

The solid−solid transformation of microporous Al_2O_3 pillared clay to sodalite could be achieved under extremely mild synthetic conditions in an ambient atmosphere. The resulting products are composed of nanometer-sized crystalline sodalite, preserving the lamellar character of the original aluminosilicates. Compared to that of hydrothermal synthesis, the nucleation and crystal growth are determined to be faster in the solid−solid transformation. The sodalite crystallization takes place by the rearrangement of delocalized sodalite nuclei formed through the solid−solid transformation, which is different from the conventional solution or amorphous-mediated processes. In addition, the present solid−solid transformation route could be applied to the preparation of nanocrystalline sodalite with a uniform particle size distribution.

Acknowledgment. This work was supported by the Korean Ministry of Science & Technology through National Research Laboratory (NRL) project 99. S. R. L. and M. P. thank the Ministry of Education for the Brain Korea 21 fellowship.

CM034614P